Asymptotic properties of radial $A + B \rightarrow C$ reaction fronts

P. M. J. Trevelyan
Faculty of Computing, Engineering and Science, University of South Wales, Pontypridd CF37 1DL, United Kingdom

A. J. Walker
School of Computing, Engineering and Physical Sciences, University of the West of Scotland, Paisley PA1 2BE, United Kingdom

(Received 16 February 2018; published 13 September 2018)

If two initially separated solutions of reactants are put in contact and a simple $A + B \rightarrow C$ reaction takes place, reaction-diffusion profiles develop due to the coupling of reaction and diffusion. The properties of such fronts are well known in the case of an initially planar contact line between the two solutions. In this study one of the reactants is injected at a constant flux from a point source into a miscible solution of the other reactant so that the reaction front expands out radially. Both the leading order large-time and small-time asymptotic limits of the reactant concentrations and reaction front position are obtained analytically. Just as in the planar reaction front case, the position of the reaction front scales like $t^{1/2}$ and the width of the reaction front scales with $t^{1/6}$. In the large Péclet number limit the large-time asymptotic properties of the radial reaction front are found to be similar to those of the planar front except that the profiles are advected with the fluid flow. The distance between the contact line and the position of the radial reaction front is $1/\sqrt{2}$ of the distance that a planar reaction front travels. Further, the length scales inside and outside of the reaction zone are reduced by factors of $2^{1/6}$ and $\sqrt{2}$, respectively, compared to the planar reaction front.

DOI: 10.1103/PhysRevE.98.032118

I. INTRODUCTION

The behavior of many chemical systems is determined by the evolution of a reaction front formed between initially separated reactants [1,2]. The simplest model of this phenomenon consists of two species A and B mixing and reacting at time $t = 0$ to form a reaction front producing species C ($A + B \rightarrow C$). When the chemical reaction changes a fluid's physical properties (density, viscosity, etc.) then convection can be induced. Experiments portraying these changes have often focused on Hele-Shaw cells [3–6].

A Hele-Shaw cell is a quasi-two-dimensional geometrical cell formed from two glass plates in which the reactive solutions are contained. One acidic solution is placed on top of another, more dense, miscible solution containing a reactant. Convective instabilities occur from double diffusive instabilities or changes in the density profile induced by chemical reaction and diffusion.

Theory and experiments on convection induced by chemical reactions have analyzed various instabilities that can deform reaction-diffusion base states [3,7–11]. Furthermore, there exist many articles considering the small- and large-time asymptotic properties of these reaction fronts in the case where the two initially separated reactants are brought into contact along a planar interface. For large times T, Venzl [12] showed that the position of the reaction front scales with $T^{\frac{1}{2}}$ when the reactants have equal diffusion coefficients. Gálfi and Rácz [13] found that the reaction zone width scaled with $T^{\frac{1}{6}}$ and the rate of production at the reaction front scaled with $T^{-\frac{2}{3}}$. The results by Gálfi and Rácz were found to be in good agreement with results from experiments conducted in gels [14,15]. These results were generalized by Koza [16] for unequal diffusion coefficients. Sinder and Pelleg were then able to obtain the solution for the product C [17]. Cornell *et al.* [18–20] were able to prove similar results for the reaction front and rate using the reaction $nA + mB \rightarrow C$. The properties of this reaction front was investigated further by Trevelyan [21]. It was found that reaction fronts could travel with different time scalings when the reactants diffuse at different rates and the initial concentration ratio is chosen appropriately.

The small-time time asymptotic properties of the reaction $A + B \rightarrow C$ are discussed by Trevelyan [22]. It can be said that these properties are not as clearly understood as the large-time counterparts. Nevertheless, Taitelbaum *et al.* found that the position and width of the reaction front and the total rate of production were found to scale with $T^{\frac{1}{2}}$ for small times [23]. Furthermore, the first-order correction to the solution was analytically expressed in terms of a double integral using the Green function for the diffusion equation. The correction to the total rate of the reaction was found to scale with $T^{\frac{3}{2}}$. Taitelbaum *et al.* also introduced approximate solutions for the small-time limit and found that the reaction front could change direction under certain conditions upon the initial concentration ratio and the ratio of the diffusion coefficients [24]. Similar approximate solutions have been found by Hecht and Taitelbaum [25]. A double-direction change was numerically found by Taitelbaum and Koza [26].

However, the bulk of the aforementioned research has focused on modeling and analyzing the reactive interface between chemicals A and B on a line or Cartesian plane. This is not an appropriate coordinate system for experiments where one wishes to inject one chemical into another, which corresponds to a single point source. Clearly, the use of a

polar coordinate system for these cases is required. Brau *et al.* studied the dynamics of $A + B \to C$ fronts by radial injection, computing the long-time evolution of the front position, its width, and production rates of the product [27]. Their work compared well with calcium carbonate precipitation experiments [28]. This problem of a localized reactant source without advection was first examined by Shipilevsky [29] in various dimensions with equal diffusion coefficients.

In this article, we consider both the small- and large-time asymptotic solutions in the case of a constant flux from a point source. Furthermore, we investigate the concentration profiles of the reaction fronts in these limits for both slow and fast flow rates. Analytical results are presented, alongside both small- and large-time asymptotics in the special case of equal diffusion coefficients. A mathematical model of the Hele-Shaw cell is presented in Sec. II, with the corresponding numerical solutions provided in Sec. III. The small- and large-time asymptotic (outer and inner) solutions are discussed in Secs. IV, V, and VI respectively. Finally, the results are discussed in Sec. VII.

II. MODEL

Consider a Hele-Shaw cell initially filled with a solution containing a reactant B at concentration B_0. At time $T = 0$ a solution containing reactant A at concentration A_0 is injected into the center of the Hele-Shaw cell through a point source. If no instabilities are present then the solution containing reactant A will spread out radially.

Upon contact, the two species react via the bimolecular reaction

$$A + B \to C \tag{1}$$

generating a product C.

The gap width h of the Hele-Shaw cell is assumed to be sufficiently small so that Darcy's law can be utilized and the domain can be considered as two-dimensional. The reactive solutions are considered sufficiently dilute so that saturation effects can be ignored and that the diffusion coefficients can be considered as constants. The resulting two-dimensional equations describing the dynamics of such a system are the following:

$$\begin{aligned}
\nabla P &= -\frac{M}{K}\underline{U},\\
\nabla \cdot \underline{U} &= 0,\\
\frac{\partial A}{\partial T} + \underline{U}\cdot\nabla A &= D_A\nabla^2 A - kAB,\\
\frac{\partial B}{\partial T} + \underline{U}\cdot\nabla B &= D_B\nabla^2 B - kAB,\\
\frac{\partial C}{\partial T} + \underline{U}\cdot\nabla C &= D_C\nabla^2 C + kAB,
\end{aligned}$$

where A, B, and C denote the concentrations of their respective species, P is the pressure, $\underline{U}$ is the velocity, M is the dynamic viscosity, $K = h^2/12$ is the permeability of the Hele-Shaw cell, k is the kinetic constant of the reaction, and D_A, D_B, and D_C are the molecular diffusion coefficients of species A, B, and C, respectively.

As we consider a radial injection, the equations are written in polar coordinates (R, θ), for which $\nabla = (\frac{\partial}{\partial R}, \frac{1}{R}\frac{\partial}{\partial \theta})$ and $\nabla^2 = \frac{1}{R}\frac{\partial}{\partial R}(R\frac{\partial}{\partial R}) + \frac{1}{R^2}\frac{\partial^2}{\partial \theta^2}$. The velocity is expressed as $\underline{U} = (U_R, U_\theta)$ to denote the radial and angular velocity components.

We introduce the following nondimensionalization:

$$t = T/T_0, \quad r = R/L_0, \quad (u, v) = (U_R, U_\theta)/U_0,$$
$$(a, b, c) = (A, B, C)/A_0, \quad \mu = M/\mu_0, \quad p = P/P_0.$$

Hence we define $P_0 = \mu_0 D_A/K$, $T_0 = 1/(kA_0)$, $L_0 = \sqrt{D_A/(kA_0)}$, and $U_0 = \sqrt{kA_0 D_A}$. Further, we define $\delta_b = D_A/D_B$ and $\delta_c = D_A/D_C$ to yield the equations

$$p_r = -\mu u, \tag{2a}$$
$$\frac{1}{r}p_\theta = -\mu v, \tag{2b}$$
$$(ru)_r + v_\theta = 0, \tag{2c}$$
$$a_t + ua_r + \frac{v}{r}a_\theta = \frac{1}{r}(ra_r)_r + \frac{a_{\theta\theta}}{r^2} - ab, \tag{2d}$$
$$b_t + ub_r + \frac{v}{r}b_\theta = \frac{1}{\delta_b}\left[\frac{1}{r}(rb_r)_r + \frac{b_{\theta\theta}}{r^2}\right] - ab, \tag{2e}$$
$$c_t + uc_r + \frac{v}{r}c_\theta = \frac{1}{\delta_c}\left[\frac{1}{r}(rc_r)_r + \frac{c_{\theta\theta}}{r^2}\right] + ab. \tag{2f}$$

In the absence of an instability of the front we can assume the problem is independent of θ with $v = 0$. Hence the flow equations depend only on the one-dimensional radial direction, so the pressure and velocity satisfy

$$\begin{aligned}
p_r &= -\mu u,\\
(ru)_r &= 0.
\end{aligned}$$

Thus u is inversely proportional to r and we write the solution as

$$u = \frac{2\mathrm{Pe}}{r}, \tag{3}$$

where u and p are undefined at $r = 0$, and at this stage, Pe is an integration constant. If μ is a constant then $p = -2\mathrm{Pe}\mu\ln(r)$.

The constant Pe can be determined by noting that the flux Q of the injected fluid is given by

$$\begin{aligned}
Q &= \int_0^{2\pi} \underline{U}\cdot\underline{e_r} R d\theta = \int_0^{2\pi} U_R R d\theta = \int_0^{2\pi} U_0 L_0 u r d\theta\\
&= \int_0^{2\pi} 2U_0 L_0 \mathrm{Pe} d\theta = 4\pi U_0 L_0 \mathrm{Pe} = 4\pi D_A \mathrm{Pe},
\end{aligned}$$

where $\underline{e_r}$ is the unit vector in the radial direction. Hence, in this problem we identify Pe as the Péclet number of the problem, defined as

$$\mathrm{Pe} = \frac{Q}{4\pi D_A}, \tag{4}$$

which measures the balance between advection and diffusion.

In the absence of diffusion, the contact line between the two liquids is an expanding circle and so the position of the contact line can be fully described by the radius of the expanding circle. Let r_c denote the position of the moving

contact line. The contact line moves at the same speed as the velocity. As the fluid velocity u is given by Eq. (3), therefore $\frac{d}{dt}r_c = u = 2\mathrm{Pe}/r_c$ at $r = r_c$. Thus $\frac{d}{dt}r_c^2 = 4\mathrm{Pe}$, and so $r_c^2 = 4\mathrm{Pe}\,t$ as $r_c = 0$ at $t = 0$. Hence, we have obtained

$$r_c = 2\sqrt{\mathrm{Pe}\,t}, \tag{5}$$

the position of the moving contact line. In dimensional variables, the position of the contact line is given by $R_c = 2\sqrt{\mathrm{Pe}D_A T} = \sqrt{QT/\pi}$.

Substituting the solution (3) for u into the system of equations (2) yields

$$a_t + (2\mathrm{Pe} - 1)\frac{a_r}{r} = a_{rr} - ab, \tag{6a}$$

$$b_t + \left(2\mathrm{Pe} - \frac{1}{\delta_b}\right)\frac{b_r}{r} = \frac{b_{rr}}{\delta_b} - ab, \tag{6b}$$

$$c_t + \left(2\mathrm{Pe} - \frac{1}{\delta_c}\right)\frac{c_r}{r} = \frac{c_{rr}}{\delta_c} + ab. \tag{6c}$$

These are the differential reaction-diffusion-advection equations that will be considered throughout the rest of the paper.

Initially the Hele-Shaw cell only contains reactant B and so, at $t = 0$, we have the initial condition

$$b = \varphi, \quad a = c = 0$$

where $\varphi = B_0/A_0$. At $r = 0$, a solution containing reactant A is being injected into the Hele-Shaw cell, therefore the boundary condition at the injection point is

$$a = 1, \quad b = c = 0 \quad \text{at } r = 0.$$

The far field boundary condition is given by

$$a \to 0, \quad b \to \varphi, \quad c \to 0 \quad \text{as } r \to \infty.$$

Introducing

$$\eta = r/\sqrt{4t}$$

and $\tau = t$ we next change from (r, t) coordinates to (η, τ) coordinates, which yields

$$\tau a_\tau - \frac{\eta}{2}a_\eta + (2\mathrm{Pe} - 1)\frac{a_\eta}{4\eta} = \frac{a_{\eta\eta}}{4} - ab\tau, \tag{7a}$$

$$\tau b_\tau - \frac{\eta}{2}b_\eta + \left(2\mathrm{Pe} - \frac{1}{\delta_b}\right)\frac{b_\eta}{4\eta} = \frac{b_{\eta\eta}}{4\delta_b} - ab\tau, \tag{7b}$$

$$\tau c_\tau - \frac{\eta}{2}c_\eta + \left(2\mathrm{Pe} - \frac{1}{\delta_c}\right)\frac{c_\eta}{4\eta} = \frac{c_{\eta\eta}}{4\delta_c} + ab\tau. \tag{7c}$$

The similarity variable η allows the initial conditions and the boundary conditions to be written together as

$$a = 1, \quad b = c = 0 \quad \text{at } \eta = 0, \tag{7d}$$

$$b \to \varphi, \quad a \to 0, \quad c \to 0 \quad \text{as } \eta \to \infty. \tag{7e}$$

Equation (7) provide the system of equations that must be numerically solved to determine the solutions for a, b, and c in η and τ coordinates. This problem depends on four parameters: Pe, φ, δ_b, and δ_c. These parameters relate to the Péclet number (Pe), the ratio of initial reactant concentrations (φ), and the ratio of molecular diffusion coefficients (δ_b and δ_c).

III. NUMERICAL SOLUTIONS

Using a Crank-Nicolson method with finite differences we can numerically solve system (6). The typical small time evolutions of the concentration profiles for a, b, and c for three values of Pe are illustrated in Fig. 1. In Fig. 1(a) the early stages of the slow flow regime are illustrated for $\mathrm{Pe} = 0.1$. We observe that species A and B have very sharp concentration

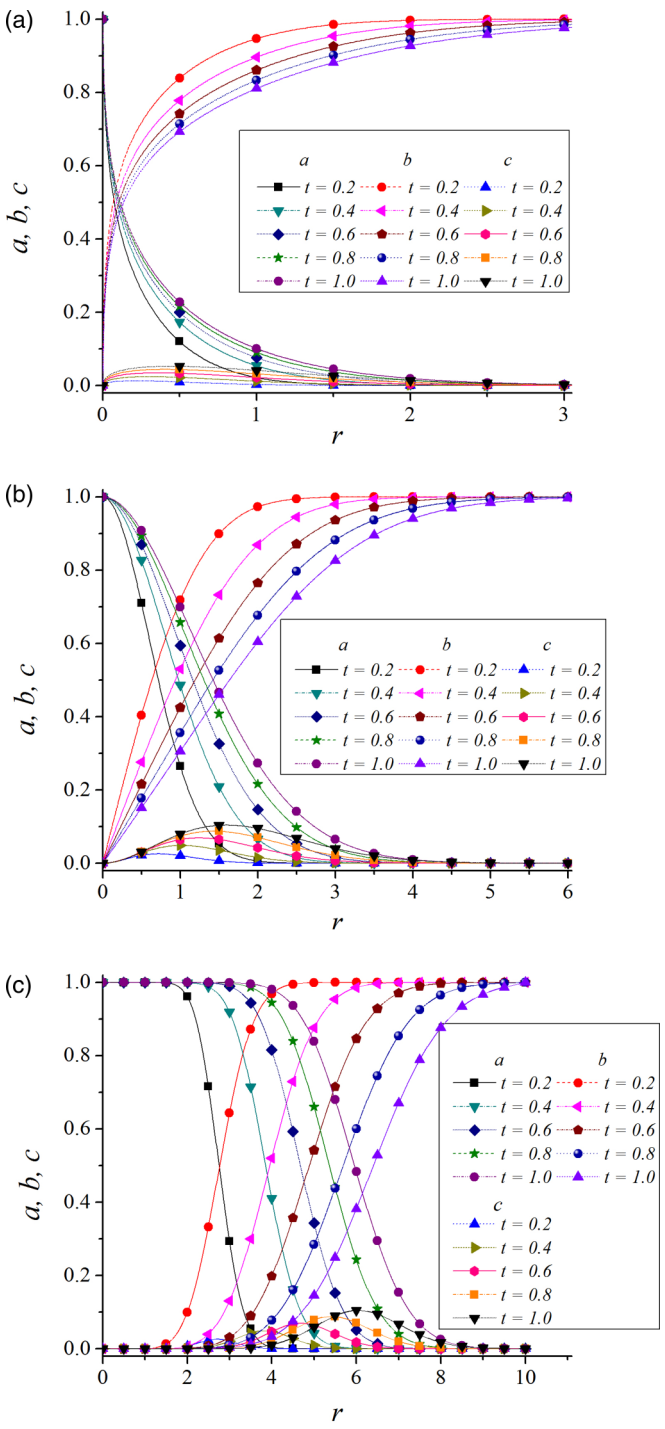

FIG. 1. Small-time concentration profiles a, b, and c are plotted against r for (a) $\mathrm{Pe} = 0.1$, (b) $\mathrm{Pe} = 1$, and (c) $\mathrm{Pe} = 10$. In each case $\delta_b = 0.5$, $\varphi = \delta_c = 1$.

gradients near $r = 0$. This is due to diffusion dominating over advection over the majority of the region, so that a boundary layer forms near $r = 0$ where species A is being injected. In Fig. 1(b) the early stages of the moderate flow regime are illustrated for Pe $= 1$. In this regime there are no boundary layers or sharp gradients as neither diffusion nor advection is dominating. In Fig. 1(c) the early stages of the fast flow regime are illustrated for Pe $= 10$. We observe that the concentration gradients of species A, B, and C are all close to zero at $r = 0$. This is due to advection dominating over diffusion so that all of the species are by transported by the fluid flow.

The typical large-time evolution of the concentration profiles for a, b, and c for three values of Pe are illustrated in Fig. 2. In Fig. 2(a) the late stages of the slow flow regime are illustrated for Pe $= 0.1$. We observe that species A, B, and C have sharp concentration gradients near $\eta = 0$. The maximum concentration of C approaches a constant and appears to move closer to $\eta = 0$ (although not illustrated, when plotted against r the local maximum in the concentration of C is found to move away from $r = 0$ at the rate $t^{1/6}$.) This is due to the local maximum in C approaching the location of the maximum reaction rate in time. Similarly, the concentration gradient of A appears to get sharper in time near $\eta = 0$, although it is actually getting less steep in time. In Fig. 2(b) the late stages of the moderate flow regime are illustrated for Pe $= 1$. In this regime both the reaction front and the maximum concentration of species C have moved away from $\eta = 0$. In Fig. 2(c) the late stages of the fast flow regime are illustrated for Pe $= 10$. In this regime the reaction front has moved sufficiently far away from the point source that the concentration gradients of A, B, and C each tend to zero away from the reaction front so that the concentration profiles resemble those associated with the planar reaction problem, but shifted to the right. Finally one notes that all of the results in Fig. 2 show the narrowing of the width of the reaction front in time when plotted against η.

IV. SMALL-TIME ASYMPTOTIC SOLUTIONS

In the limit as τ tends to zero the leading-order transport equations in (7) for the reactants become

$$-2\eta a_\eta + (2\mathrm{Pe} - 1)\frac{a_\eta}{\eta} = a_{\eta\eta}, \tag{8a}$$

$$-2\delta_b \eta b_\eta + (2\delta_b \mathrm{Pe} - 1)\frac{b_\eta}{\eta} = b_{\eta\eta} \tag{8b}$$

with $c = O(\tau)$. Thus, to leading order, there is no product. The general solution to (8) take the form

$$a = d_1 + d_2\Gamma(\mathrm{Pe}, \eta^2), \quad b = d_3 + d_4\Gamma(\delta_b \mathrm{Pe}, \delta_b \eta^2)$$

where Γ is the incomplete Gamma function defined by

$$\Gamma(a, z) = \int_z^\infty x^{a-1} e^{-x} dx;$$

see Eq. (6.5.3) in [30]. Note that the solution can also be written in terms of Whittaker's functions [31]. Using the four

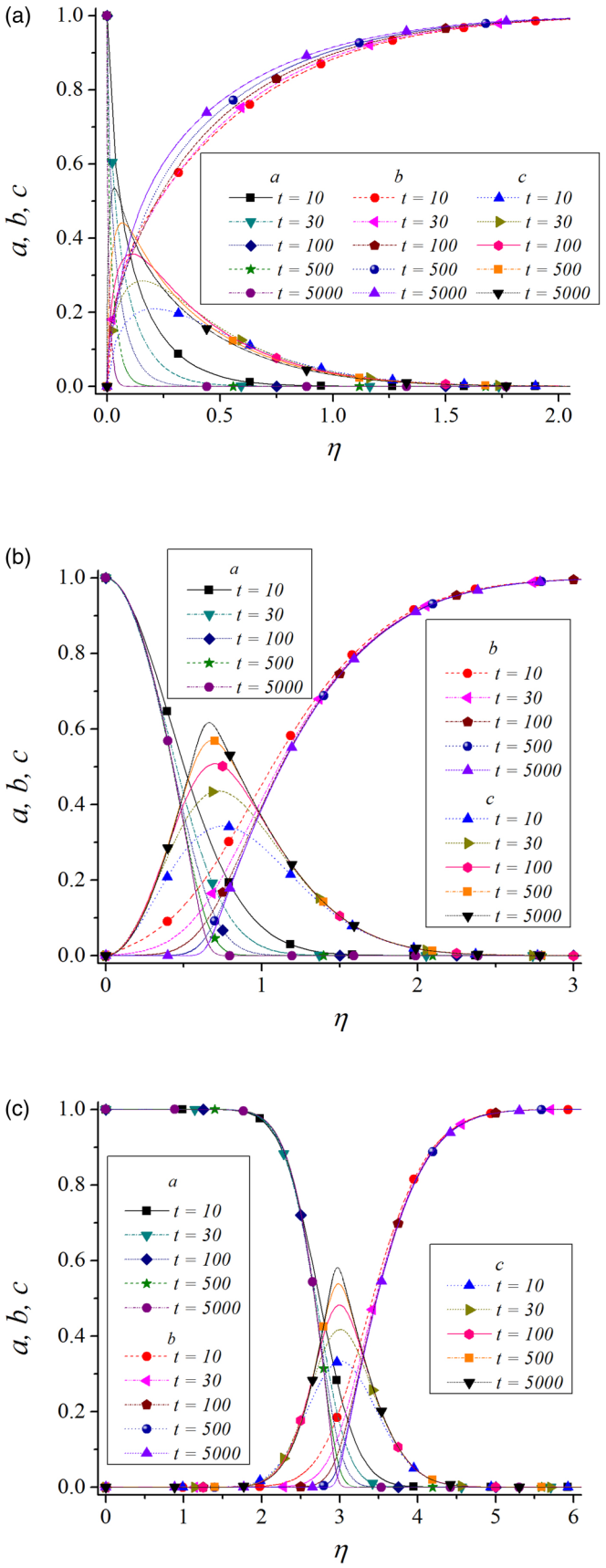

FIG. 2. Large-time concentration profiles a, b, and c are plotted against η for (a) Pe $= 0.1$, (b) Pe $= 1$, and (c) Pe $= 10$. In each case $\delta_b = 0.5$, $\varphi = \delta_c = 1$.

boundary conditions (7d) and (7e) leads to the solutions

$$a = \frac{\Gamma(\mathrm{Pe}, \eta^2)}{\Gamma(\mathrm{Pe})}, \tag{9a}$$

$$b = \varphi - \varphi \frac{\Gamma(\delta_b \mathrm{Pe}, \delta_b \eta^2)}{\Gamma(\delta_b \mathrm{Pe})}, \tag{9b}$$

where $\Gamma(x) = \Gamma(0, x)$. Now that the leading-order analytical solutions have been determined in the small-time asymptotic limit we can obtain some physical properties of the system.

A. Maximum reaction rate

We define the reaction rate as kab. The initial position of the reaction rate can be described as the point where the reaction rate is maximum, i.e., at $(kab)_\eta = 0$. Using the small-time asymptotic solutions in Eq. (9) the maximum reaction rate is found to occur at

$$r_m = 2\beta\sqrt{t}, \tag{10}$$

where β is the solution to the equation

$$\frac{\Gamma(\delta_b \mathrm{Pe}) - \Gamma(\delta_b \mathrm{Pe}, \delta_b \beta^2)}{\Gamma(\mathrm{Pe}, \beta^2)} = \delta_b^{\delta_b \mathrm{Pe}} \beta^{2\mathrm{Pe}(\delta_b - 1)} e^{(1-\delta_b)\beta^2}. \tag{11}$$

Equivalently, the maximum reaction rate occurs at $\eta = \beta$. We note that, in dimensional quantities, the position where the reaction rate is maximum is given by $R_m = 2\beta\sqrt{D_A T}$.

By numerically solving Eq. (11), the dependence of β on δ_b can be determined, and is illustrated in Fig. 3 for various values of Pe. In Fig. 3(a), we observe that increasing Pe increases β; however, β has a nonmonotonic dependence on δ_b, just as in the planar reaction front case. In Fig. 3(b), we notice that $\beta - \sqrt{\mathrm{Pe}}$ is a nonmonotonic function of both Pe and δ_b, and thus so is the distance between the local maximum in the reaction rate and the contact line, as $r_m - r_c = 2\sqrt{t}(\beta - \sqrt{\mathrm{Pe}})$. In the following subsections some limits are examined and additional properties of the reaction front are presented.

B. Equal diffusion coefficients

If both reactants diffuse at the same rate, i.e., $\delta_b = 1$, then Eq. (11) simplifies to

$$\frac{\Gamma(\mathrm{Pe}, \beta^2)}{\Gamma(\mathrm{Pe})} = \frac{1}{2}, \tag{12}$$

which reveals that β is a monotonic increasing function of Pe. This result is physically expected as increasing the flow rate increases the propagation of the reaction front. Using Eq. (B1) in Appendix B, in the large-Pe limit we obtain

$$\beta \to \sqrt{\mathrm{Pe}} - \frac{1}{6\sqrt{\mathrm{Pe}}} + O(\mathrm{Pe}^{-3/2}) \tag{13}$$

so that the position of the reaction front quickly approaches the contact line.

C. Slow flow rate

In the slow flow rate limit, i.e., Pe tending to zero, we shall also consider β small and δ_b up to order unity. Using Eqs. (A1) and (A2) in Appendix A we can expand Eq. (11) to first order in Pe and β to obtain

$$\beta \to \left(\frac{\delta_b \Gamma(\mathrm{Pe} + 1)}{1 + \delta_b} \right)^{1/(2\mathrm{Pe})}, \tag{14}$$

which tends to zero very quickly. This equation reveals that increasing δ_b or Pe lead to an increase in β. This asymptotic analytical solution (14) is illustrated by the dotted lines in Fig. 3(a) and is found to be in good agreement with the numerical solution of Eq. (11) when both Pe and β are small. If $\delta_b \gg 1$ then β may no longer be small and then the limit fails.

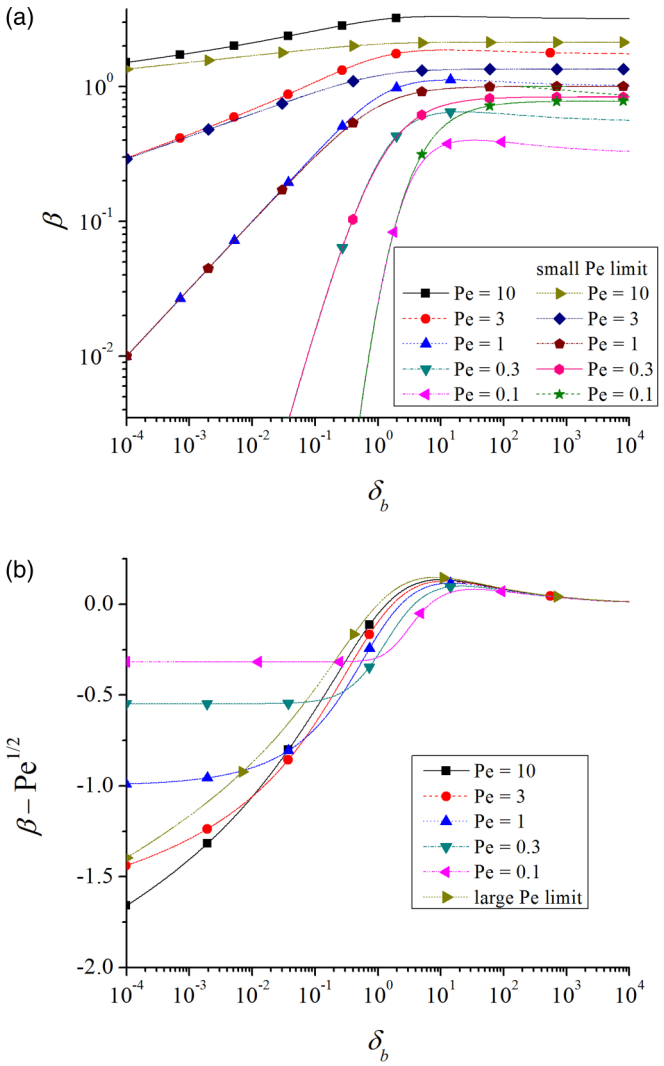

FIG. 3. The relationship between β and δ_b for various values of Pe obtained from Eq. (11). In (a) (δ_b) is plotted against (β) where the second set of lines denote the small-Pe limit given analytically by Eq. (14). In (b) (δ_b) is plotted against $\beta - \sqrt{\mathrm{Pe}}$ where the short-dotted line denotes the large Pe limit determined from Eq. (15).

D. Fast flow rate

In the fast flow rate limit, i.e., Pe tending to infinity, we choose a variable proportional to the distance between the reaction zone and the contact line by writing $\chi = \sqrt{2}(\beta -$

$\sqrt{Pe}$). Using the zeroth-order term from Eqs. (B1) and (B2) in Appendix B along with $e^{-xyz}(1+x/z)^{yz^2} \to e^{-yx^2/2}$ as z tends to infinity, Eq. (11) becomes

$$e^{(\delta_b-1)\chi^2}\mathrm{erfc}(-\sqrt{\delta_b}\chi) = \sqrt{\delta_b}\mathrm{erfc}(\chi) \tag{15}$$

to leading order. In Fig. 3(b) the numerical solution to χ from Eq. (15) allows the determination of β and is illustrated by the dotted lines. For large Pe, this solution is found to be in good agreement with the numerical solution of (11) when δ_b is not too small.

We note that Eq. (15) is the same equation as for planar reaction fronts obtained by Koza [16] in the small-time asymptotic limit. Thus we have shown that $r_m = r_c + x_m/\sqrt{2}$ where x_m is the location where the reaction rate is maximum for a planar reaction front. Using the properties of Eq. (15) we find that

$$\beta \to \sqrt{\mathrm{Pe}} + \frac{\sqrt{\pi}(\sqrt{\delta_b}-1)}{4\sqrt{2\delta_b}}$$

for $|\delta_b - 1| \ll 1$, so that the reaction front is only ahead of the contact line when $\delta_b > 1$. Further, one finds that the position of the reaction front varies nonmonotonically with δ_b, such that the reaction front extends furthest ahead of the contact line when $\delta_b = \delta_b^{(c)} \approx 8.056588$, in dimensionless variables. In dimensional variables this means that, for a fixed value of D_A, the reaction fronts extends furthest ahead of the contact line when $D_B = D_A/\delta_b^{(c)}$, and by symmetry, for a fixed value of D_B, the reaction front lags furthest behind the contact line when $D_B = \delta_b^{(c)} D_A$.

E. Reaction front at contact line

When the reaction front is located at the contact line we have $\beta = \sqrt{\mathrm{Pe}}$ and Eq. (11) becomes

$$\frac{\Gamma(\delta_b\mathrm{Pe}) - \Gamma(\delta_b\mathrm{Pe}, \delta_b\mathrm{Pe})}{\Gamma(\mathrm{Pe}, \mathrm{Pe})} = \delta_b^{\delta_b\mathrm{Pe}}(\mathrm{Pe}/e)^{\mathrm{Pe}(\delta_b-1)}. \tag{16}$$

By numerically solving Eq. (16) the parameter values of Pe and δ_b required for the initial reaction front to be located at the fluid contact line are obtained, and they are plotted in Fig. 4. We notice that if δ_b is greater than a critical value greater than unity and depending on Pe, then $\beta^2 > \mathrm{Pe}$ and the reaction front will travel ahead of the contact line. Thus when $\delta_b < 1$, then $\beta < \sqrt{\mathrm{Pe}}$ for all $\mathrm{Pe} > 0$. Increasing Pe is found to increase β and reduces the critical value of δ_b required for which $\beta = \sqrt{Pe}$. Below this critical value of δ_b, increasing δ_b increases β, while above this value β has the same type of nonmonotonic dependence on δ_b as found in planar reaction fronts.

Using Eqs. (A1) and (A2) in Appendix A, we find that as Pe tends to zero we require that δ_b tends to infinity in order to maintain the reaction front at the contact line. Keeping the most dominant terms in the expansion, we obtain

$$\delta_b \to -\frac{1}{\mathrm{Pe}\ln(\mathrm{Pe})}, \tag{17a}$$

which is in reasonable agreement with the numerical solution to Eq. (16); see Fig. 4.

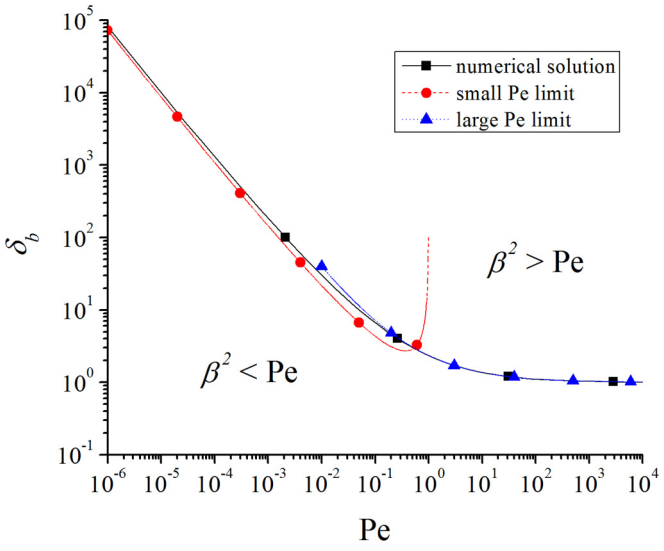

FIG. 4. The condition for the initial reaction front to be located at the fluid contact line in the (δ_b, Pe) parameter space, obtained from Eq. (16). The dashed and dotted lines are the small and large Pe limits given by Eqs. (17a) and (17b), respectively.

In the fast flow rate limit, taking $\mathrm{Pe} \to \infty$ and using Eqs. (B1) and (B2) in Appendix B yields

$$\delta_b \to 1 + \frac{4\sqrt{2}}{3\sqrt{\pi\mathrm{Pe}}} + \frac{8}{9\pi\mathrm{Pe}} + \cdots, \tag{17b}$$

which is found to be in very good agreement with the numerical solution to Eq. (16) as shown in Fig. 4.

F. First moment of the reaction rate

In the previous section the small-time asymptotic location of the position where the reaction rate has a maximum was analyzed. Another interesting case to examine is the first moment of the reaction rate. In radial coordinates this definition becomes

$$r_f = \frac{\int_0^\infty abr^2 dr}{\int_0^\infty abr\, dr} = 2\sqrt{t}\frac{\int_0^\infty ab\eta^2 d\eta}{\int_0^\infty ab\eta\, d\eta}. \tag{18}$$

Using the small time asymptotic profiles in Eq. (9) we can obtain r_f; see Fig. 5(a).

Figure 5(a) shows that r_f is a monotonic increasing function of both δ_b and Pe. Figure 5(b) shows that the term $r_f - r_c$ is a monotonic increasing function of δ_b and it is a monotonic decreasing function of Pe. We note that r_f can be expressed analytically in terms of hypergeometric functions, but here we will only present it analytically in the fast flow rate limit.

In the fast flow rate regime, using Eq. (B1), the solutions in Eq. (9), to second order, are given by

$$a = \frac{\mathrm{erfc}(\xi)}{2} + \frac{e^{-\xi^2}}{6\sqrt{\pi}}\left[\frac{\xi^2-2}{\sqrt{2\mathrm{Pe}}} + \frac{6\xi - 8\xi^3 + \xi^5}{12\mathrm{Pe}}\right], \tag{19a}$$

$$b = \frac{\varphi\,\mathrm{erfc}(-\sqrt{\delta_b}\xi)}{2} - \frac{\varphi e^{-\delta_b\xi^2}}{6\sqrt{\pi\delta_b}}\left[\frac{\delta_b\xi^2-2}{\sqrt{2\mathrm{Pe}}} + \frac{6\xi - 8\delta_b\xi^3 + \delta_b^2\xi^5}{12\mathrm{Pe}}\right], \tag{19b}$$

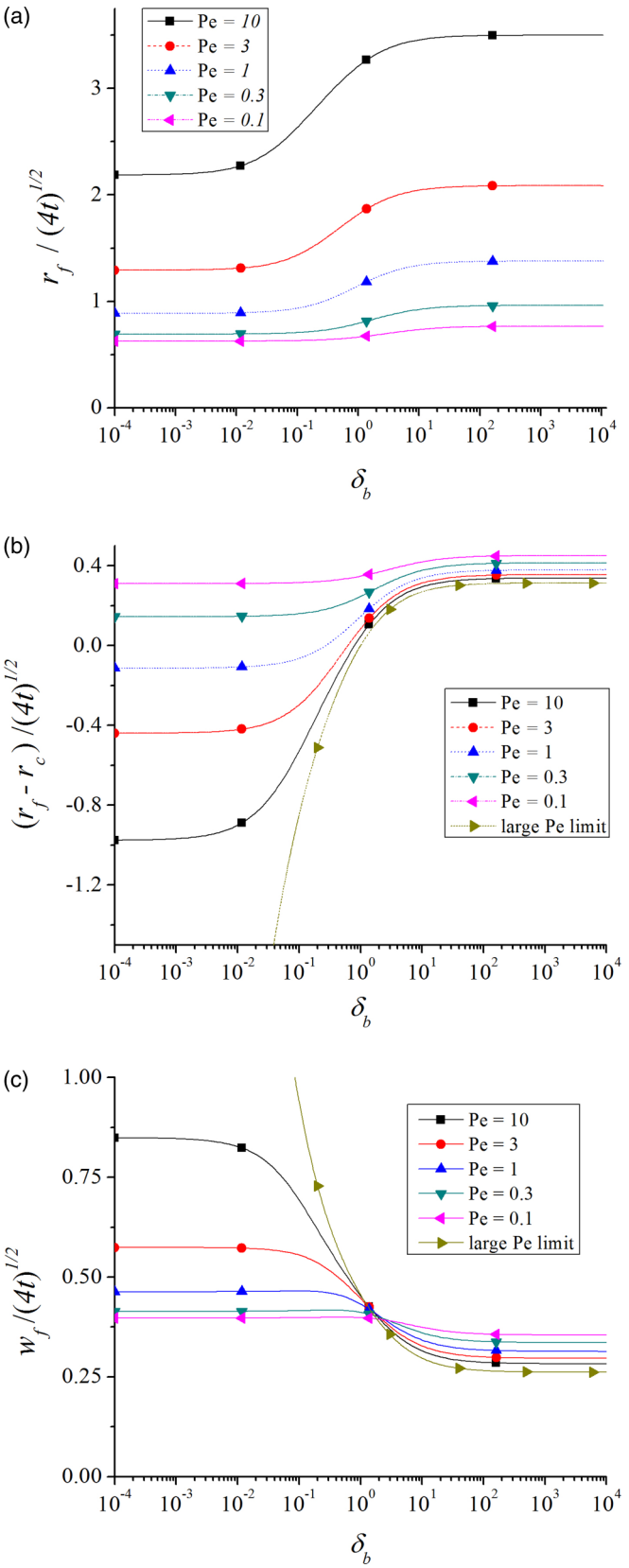

FIG. 5. The relationship between small-time asymptotic values of (a) r_f, (b) $r_f - r_c$, and (c) w_f with δ_b for various values of Pe. The short-dotted line in (b) is the large-Pe limit of $r_f - r_c$ given by Eq. (20) and in (c) the short-dotted line is the large-Pe limit of w_f given by Eq. (22).

where $\xi = \sqrt{2}(\eta - \sqrt{\mathrm{Pe}})$. Substituting these solutions into Eq. (18) and expanding in large Pe allows r_f to be asymptotically expanded as

$$r_f \to 2\sqrt{\mathrm{Pe}t} + \frac{\sqrt{\pi t}(\delta_b - 1)}{2\sqrt{2\delta_b(1+\delta_b)}} + O(\mathrm{Pe}^{-1/2}) \qquad (20)$$

to leading order, where the integral results in [22] have been used. One notes that r_f monotonically increases with δ_b, unlike r_m, and r_f coincides with the location of the contact line r_c when $\delta_b = 1$. Additionally, we have obtained $r_f = r_c + x_f/\sqrt{2}$, where x_f is the solution given by Eq. (16) in [22].

G. Width of the reaction front

The width of the reaction front is generally obtained using the second moment of the reaction rate. Here we define the width of the reaction front w_f, to satisfy

$$w_f^2 = \frac{\int_0^\infty ab(r - r_f)^2 r dr}{\int_0^\infty abr\, dr} = \frac{\int_0^\infty abr^3 dr}{\int_0^\infty abr\, dr} - r_f^2$$
$$= 4t\frac{\int_0^\infty ab\eta^3 d\eta}{\int_0^\infty ab\eta d\eta} - r_f^2. \qquad (21)$$

Using the small-time asymptotic profiles in Eq. (9) we can obtain w_f, see Fig. 5(c), which shows that w_f is a monotonic decreasing function of δ_b, but surprisingly the effect of Pe is nonmonotonic. If δ_b is large then increasing Pe reduces w_f; however, if δ_b is small then increasing Pe increases w_f. Similarly, we can express w_f analytically in terms of hypergeometric functions, but here we will just present the solution in the fast flow rate limit.

Substituting the solutions in Eq. (19) into Eq. (21) and expanding in large Pe allows w_f to be asymptotically expanded as

$$w_f^2 \to \frac{t}{\delta_b + 1}\left[\left(\frac{1}{\delta_b} + \delta_b\right)\left(\frac{2}{3} - \frac{\pi}{8}\right) + \frac{1}{3} + \frac{\pi}{4}\right] \qquad (22)$$

to leading order. This expression for w_f^2 is exactly $\frac{1}{2}$ of the value one obtains for a planar reaction front; see Eq. (18) in [22], and thus the small-time asymptotic width of a radial reaction front in the large Pe limit is $1/\sqrt{2}$ of the width of the corresponding planar reaction front.

H. Summary of small-time asymptotic properties

We have found that increasing Pe has a monotonic increasing effect on both r_m and r_f, a monotonic decreasing effect on $r_f - r_c$, and a nonmonotonic effect on $r_m - r_c$ and w_f. The parameter δ_b has a monotonic increasing effect on r_f and $r_f - r_c$, a monotonic decreasing effect on w_f, and a nonmonotonic effect on r_m and $r_m - r_c$. These results are summarized in Table I.

Finally we note that increasing δ_b or increasing Pe, when $\delta_b > 1$, sufficiently lead to $r_m > r_c$. Now that the various properties of the small-time asymptotic solutions have been obtained, in the next section the properties of the large-time asymptotic solutions will be examined.

TABLE I. Parameter effects upon the small-time asymptotic properties of the reaction front.

Parameter	r_m	$r_m - r_c$	r_f	$r_f - r_c$	w_f
δ_b	$\pm$	$\pm$	$+$	$+$	$-$
Pe	$+$	$\pm$	$+$	$-$	$\pm$

V. LARGE-TIME ASYMPTOTIC OUTER SOLUTIONS

In the large-time limit, we seek a similarity solution outside the reaction zone where the solution does not depend on τ and $ab = 0$, i.e., away from the reaction front, which we name the outer solution. These assumptions reduce the equations in (7) to

$$-2\eta a_\eta + (2\mathrm{Pe} - 1)\frac{a_\eta}{\eta} = a_{\eta\eta}, \tag{23a}$$

$$-2\delta_b \eta b_\eta + (2\delta_b \mathrm{Pe} - 1)\frac{b_\eta}{\eta} = b_{\eta\eta}, \tag{23b}$$

$$-2\delta_c \eta c_\eta + (2\delta_c \mathrm{Pe} - 1)\frac{c_\eta}{\eta} = c_{\eta\eta}. \tag{23c}$$

We assume that the reaction front is located at

$$r_f = 2\alpha\sqrt{t}, \tag{24}$$

which is equivalent to $\eta = \alpha$. We now introduce the superscript notation 1 and 2 to denote the outer solution behind and ahead of the reaction front, respectively. At the reaction front we suppose that

$$a^{(1)} = b^{(2)} = 0, \quad c^{(1)} = c^{(2)} = W \quad \text{at } \eta = \alpha.$$

Using these four boundary conditions along with Eqs. (7d) and (7e) yields the solutions

$$a^{(1)} = \frac{\Gamma(\mathrm{Pe}, \eta^2) - \Gamma(\mathrm{Pe}, \alpha^2)}{\Gamma(\mathrm{Pe}) - \Gamma(\mathrm{Pe}, \alpha^2)}, \quad b^{(1)} = 0, \tag{25a}$$

$$b^{(2)} = \varphi - \varphi\frac{\Gamma(\delta_b \mathrm{Pe}, \delta_b \eta^2)}{\Gamma(\delta_b \mathrm{Pe}, \delta_b \alpha^2)}, \quad a^{(2)} = 0, \tag{25b}$$

$$c^{(1)} = W\frac{\Gamma(\delta_c \mathrm{Pe}) - \Gamma(\delta_c \mathrm{Pe}, \delta_c \eta^2)}{\Gamma(\delta_c \mathrm{Pe}) - \Gamma(\delta_c \mathrm{Pe}, \delta_c \alpha^2)}, \tag{25c}$$

$$c^{(2)} = W\frac{\Gamma(\delta_c \mathrm{Pe}, \delta_c \eta^2)}{\Gamma(\delta_c \mathrm{Pe}, \delta_c \alpha^2)}. \tag{25d}$$

However, the values of α and W have not yet been determined. These quantities are obtained by matching the reactant fluxes across the reaction zone, namely, using

$$-\frac{\partial a^{(1)}}{\partial \eta} = \frac{1}{\delta_b}\frac{\partial b^{(2)}}{\partial \eta} = \frac{1}{\delta_c}\frac{\partial (c^{(1)} - c^{(2)})}{\partial \eta} \quad \text{at } \eta = \alpha. \tag{26}$$

By writing

$$U = -\frac{\partial a^{(1)}}{\partial \eta} = \frac{2\alpha^{2\mathrm{Pe}-1}e^{-\alpha^2}}{\Gamma(\mathrm{Pe}) - \Gamma(\mathrm{Pe}, \alpha^2)},$$

$$V = \frac{\partial b^{(2)}}{\partial \eta} = \frac{2\varphi\delta_b^{\delta_b \mathrm{Pe}}\alpha^{2\delta_b \mathrm{Pe}-1}e^{-\delta_b\alpha^2}}{\Gamma(\delta_b \mathrm{Pe}, \delta_b \alpha^2)},$$

$$W_L = \frac{\partial c^{(1)}}{\partial \eta} = \frac{2W\delta_c^{\delta_c \mathrm{Pe}}\alpha^{2\delta_c \mathrm{Pe}-1}e^{-\delta_c\alpha^2}}{\Gamma(\delta_c \mathrm{Pe}) - \Gamma(\delta_c \mathrm{Pe}, \delta_c \alpha^2)},$$

$$W_R = -\frac{\partial c^{(2)}}{\partial \eta} = \frac{2W\delta_c^{\delta_c \mathrm{Pe}}\alpha^{2\delta_c \mathrm{Pe}-1}e^{-\delta_c\alpha^2}}{\Gamma(\delta_c \mathrm{Pe}, \delta_c \alpha^2)},$$

Eq. (26) becomes

$$U = \frac{V}{\delta_b} = \frac{W_R + W_L}{\delta_c},$$

which leads to the equations

$$\frac{\Gamma(\delta_b \mathrm{Pe}, \delta_b \alpha^2)}{\Gamma(\mathrm{Pe}) - \Gamma(\mathrm{Pe}, \alpha^2)} = \varphi\delta_b^{\delta_b \mathrm{Pe}-1}\alpha^{2\mathrm{Pe}(\delta_b-1)}e^{\alpha^2(1-\delta_b)} \tag{27}$$

and

$$W = \frac{\Gamma(\delta_c \mathrm{Pe}, \delta_c \alpha^2)[\Gamma(\delta_c \mathrm{Pe}) - \Gamma(\delta_c \mathrm{Pe}, \delta_c \alpha^2)]}{\Gamma(\delta_c \mathrm{Pe})[\Gamma(\mathrm{Pe}) - \Gamma(\mathrm{Pe}, \alpha^2)]} \times \alpha^{2\mathrm{Pe}(1-\delta_c)}e^{\alpha^2(\delta_c-1)}\delta_c^{1-\delta_c \mathrm{Pe}}. \tag{28}$$

Thus, once Eq. (27) has been solved, W and hence the outer solution have been determined.

By numerically solving Eq. (27), the dependence of α on δ_b, Pe and φ can be determined. In Fig. 6 the variation of α with δ_b is illustrated for various values of Pe when $\varphi = 1$. In Fig. 6(a), we observe that increasing Pe or δ_b increases α. In Fig. 6(b), we notice that the distance between the reaction front and the contact line, i.e., $r_f - r_c = 2\sqrt{t}(\alpha - \sqrt{\mathrm{Pe}})$, is a monotonic increasing function of δ_b and a nonmonotonic function of Pe.

In Fig. 7 the variation of α with δ_b is illustrated for various values of φ when $\mathrm{Pe} = 1$. We observe that decreasing φ or increasing δ_b increases α. In the following subsections some interesting limits are examined and additional properties of the reaction front are presented.

A. Equal diffusion coefficients

If both reactants diffuse at the same rate so that $\delta_b = 1$ then Eq. (27) reduces to

$$\frac{\varphi}{1+\varphi} = \frac{\Gamma(\mathrm{Pe}, \alpha^2)}{\Gamma(\mathrm{Pe})}, \tag{29}$$

which reveals that α is a monotonic decreasing function of φ. Further, an expansion in large Pe yields

$$\alpha \to \sqrt{\mathrm{Pe}} + \frac{1}{\sqrt{2}}\mathrm{erfc}^{-1}\left(\frac{2\varphi}{1+\varphi}\right), \tag{30}$$

which is found to be in good agreement with numerical solutions to Eq. (29) when Pe is large.

B. Slow flow rate

Letting Pe tend to zero and assuming that α is small with φ and δ_b both being $O(1)$, to leading order yields

$$\alpha \to \frac{1}{\sqrt{\delta_b}}\left(\frac{\Gamma(\delta_b \mathrm{Pe} + 1)}{\varphi + 1}\right)^{1/(2\delta_b \mathrm{Pe})}, \tag{31}$$

which tends to zero very quickly as Pe tends to zero. This analytical solution (31) is illustrated by the dotted lines in Fig. 6(a) and is found to be in good agreement with the actual numerical solution when both Pe and α are small; however, the approximation is not valid when the term $\mathrm{Pe}\delta_b$ becomes large, as the approximation predicts that α has a nonmonotonic

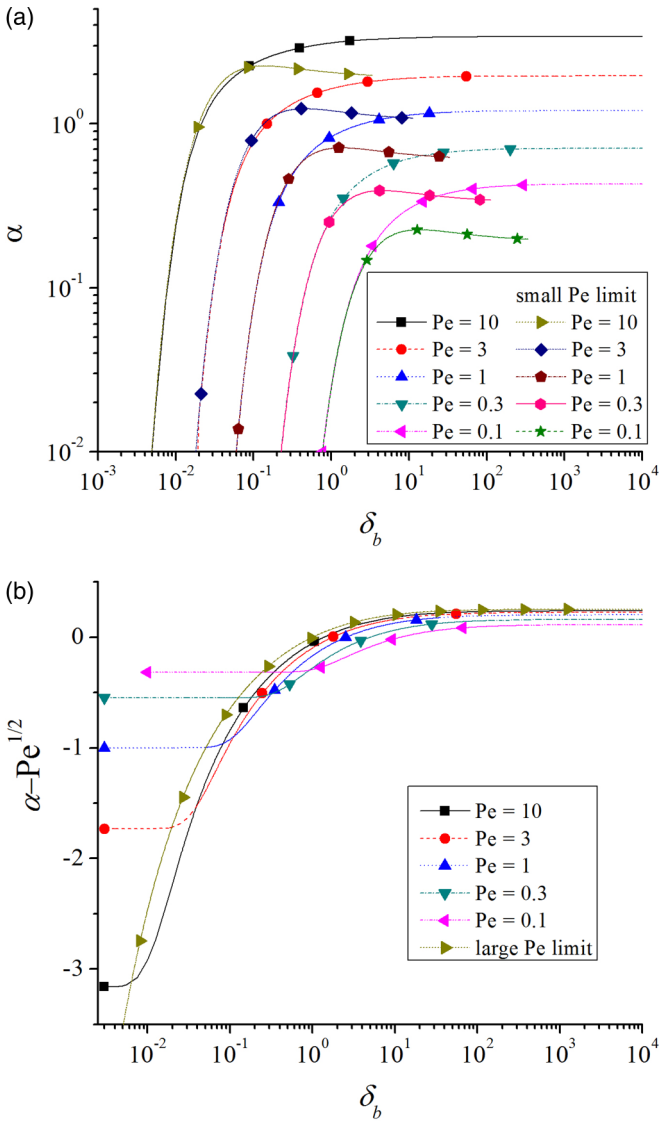

FIG. 6. The relationship between α and δ_b for various values of Pe obtained from Eq. (27) when $\varphi = 1$. In (a) (δ_b) is plotted against (α), where the second set of lines denote the small-Pe limit given by Eq. (31). In (b) (δ_b) is plotted against $\alpha - \sqrt{\text{Pe}}$, where the short-dotted line denotes the large-Pe limit determined from Eq. (32).

dependence on δ_b but the actual solution shows that increasing δ_b causes a monotonic increase in α.

In Fig. 7 we find that the approximation can be good even when Pe is not small, when $\delta_b \ll 1$; however, if φ is small then the approximation starts to diverge from the the numerical solution at smaller values of δ_b.

C. Fast flow rate

Letting Pe tend to infinity allows Eq. (27) to be reduced to the same equation as for planar reaction fronts obtained by Koza [16]. By writing $\psi = \sqrt{2}(\alpha - \sqrt{\text{Pe}})$, to leading order, we obtain

$$e^{(\delta_b-1)\psi^2}\text{erfc}(\sqrt{\delta_b}\psi) = \frac{\varphi}{\sqrt{\delta_b}}\text{erfc}(-\psi), \tag{32}$$

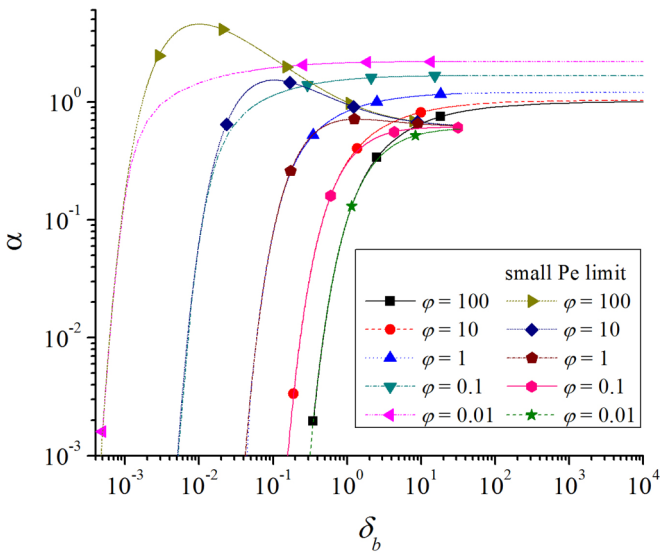

FIG. 7. The relationship between α and δ_b for various values of φ obtained from Eq. (27) when Pe = 1. The second set of lines denote the small-Pe limit by Eq. (31).

whose properties have already been studied in the literature for the planar reaction front.

In Fig. 6(b) the numerical solution to ψ from Eq. (32) allows the determination of α and is illustrated by the dotted line. For large Pe, this solution is found to be in good agreement with the numerical solution of (27) when δ_b is not too small.

D. Reaction front at contact line

When the reaction front is located at the contact line we have $\alpha = \sqrt{\text{Pe}}$, and Eq. (27) becomes

$$\frac{\Gamma(\delta_b\text{Pe}, \delta_b\text{Pe})}{\Gamma(\text{Pe}) - \Gamma(\text{Pe}, \text{Pe})} = \varphi\delta_b^{\delta_b\text{Pe}-1}(\text{Pe}/e)^{\text{Pe}(\delta_b-1)}. \tag{33}$$

By numerically solving Eq. (33) the parameter values of Pe and δ_b required for the large-time asymptotic position of the reaction front to be located at the fluid contact line are obtained for various values of φ, and they are plotted in Fig. 8. We notice that if δ_b is greater than a critical value greater than $1/\varphi^2$ and depending on Pe, then $\alpha^2 > \text{Pe}$ and the reaction front will travel ahead of the contact line. Thus when $\delta_b < \varphi$, then $\alpha < \sqrt{\text{Pe}}$ for all Pe > 0. Increasing Pe is found to increase α and reduce the critical value of δ_b required for which $\alpha = \sqrt{\text{Pe}}$.

Using Eqs. (A1) and (A2) in Appendix A, we find that, as Pe tends to zero, we require that δ_b tends to infinity in order to maintain the reaction front at the contact line. Keeping the most dominant terms in the expansion, we obtain $\varphi \to e^{\delta_b\text{Pe}}(\delta_b\text{Pe})^{1-\delta_b\text{Pe}}\Gamma(\delta_b\text{Pe}, \delta_b\text{Pe})$. If $\varphi \gg 1$ and Pe tends to zero then we find that

$$\delta_b \to \frac{2}{\pi\text{Pe}}\left(\varphi + \frac{1}{3}\right)^2, \tag{34a}$$

which is in reasonable agreement with the numerical solution to Eq. (33) (see Fig. 8), when Pe is small.

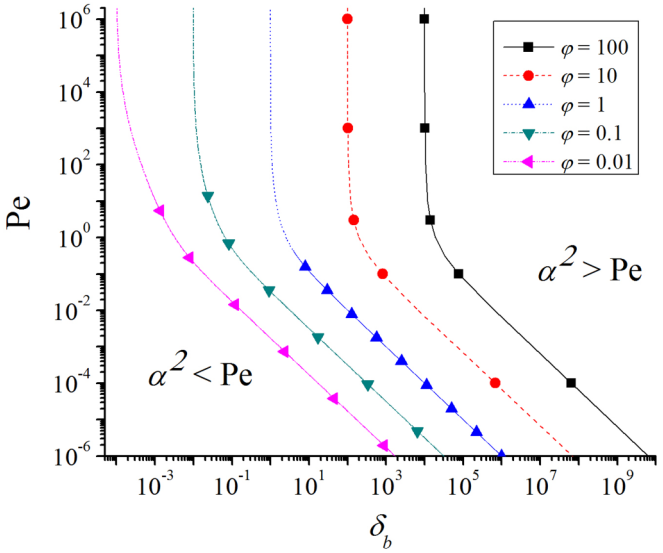

FIG. 8. The condition for the large-time asymptotic position of the reaction front to be located at the fluid contact line in the (δ_b, Pe) parameter space for various values of φ, obtained from Eq. (33).

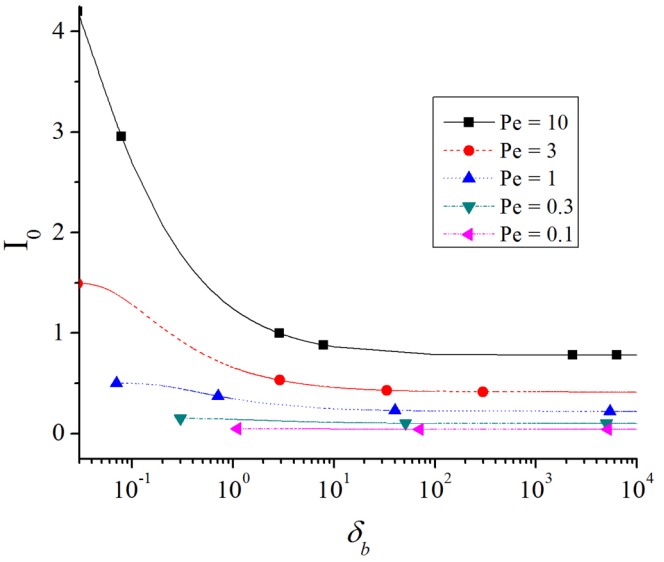

FIG. 9. The relationship between the total amount of the product I_0 and δ_b for various values of Pe with $\varphi = 1$.

In the fast flow rate limit, taking $\mathrm{Pe} \to \infty$ and using Eqs. (B1) and (B2) in Appendix B yields

$$\varphi = \sqrt{\delta_b} - \frac{\sqrt{2}(1+\sqrt{\delta_b})}{3\sqrt{\pi\,\mathrm{Pe}}} + \frac{1+\sqrt{\delta_b}}{9\pi\,\mathrm{Pe}} + \frac{\delta_b - 1}{12\sqrt{\delta_b}\,\mathrm{Pe}}, \quad (34b)$$

which is found to be in very good agreement with the numerical solution to Eq. (33), as shown in Fig. 8, when Pe is large. The first term of Eq. (34b) is $\varphi = \sqrt{\delta_b}$ which is equivalent to the condition obtained by Koza [16] for the case of a stationary planar reaction front, namely

$$\frac{B_0\sqrt{D_B}}{A_0\sqrt{D_A}} = 1.$$

E. Total amount of the product

The total amount of product produced in dimensional quantities is

$$C_{\mathrm{total}} = \int_0^{2\pi}\int_0^{\infty} C\,R\,dR\,d\theta = 2\pi A_0 L_0^2 \int_0^{\infty} cr\,dr$$
$$= 8\pi A_0 L_0^2 t \int_0^{\infty} c\eta\,d\eta = 8\pi A_0 D_A T I_0$$

so that the production rate is linear in time where

$$I_0 = \int_0^{\infty} c\eta\,d\eta.$$

This can be evaluated using the large-time asymptotic solutions for c_1 and c_2 in (25). Using

$$\int_0^x \Gamma(a,z)dz = (x-a)\Gamma(a,x) - x^a e^{-x} + \Gamma(a+1)$$

we find that

$$I_0 = \int_0^{\infty} c\eta\,d\eta = \frac{e^{-\alpha^2}\alpha^{2\mathrm{Pe}}}{2[\Gamma(\mathrm{Pe}) - \Gamma(\mathrm{Pe},\alpha^2)]} = \frac{U\mathrm{Pe}}{4}.$$

If α is considered fixed then the production rate increases as Pe is increased. If Pe is considered fixed then the production rate decreases as α is increased.

Returning to dimensional quantities, we have

$$C_{\mathrm{total}} = \frac{4\pi A_0 D_A T e^{-\alpha^2}\alpha^{2\mathrm{Pe}}}{\Gamma(\mathrm{Pe}) - \Gamma(\mathrm{Pe},\alpha^2)} = \frac{A_0 U Q T}{2}. \quad (35)$$

We plot the total amount of the product against δ_b for various values of Pe when $\varphi = 1$ in Fig. 9 and the total amount of the product against δ_b for various values of φ when Pe = 1 in Fig. 10.

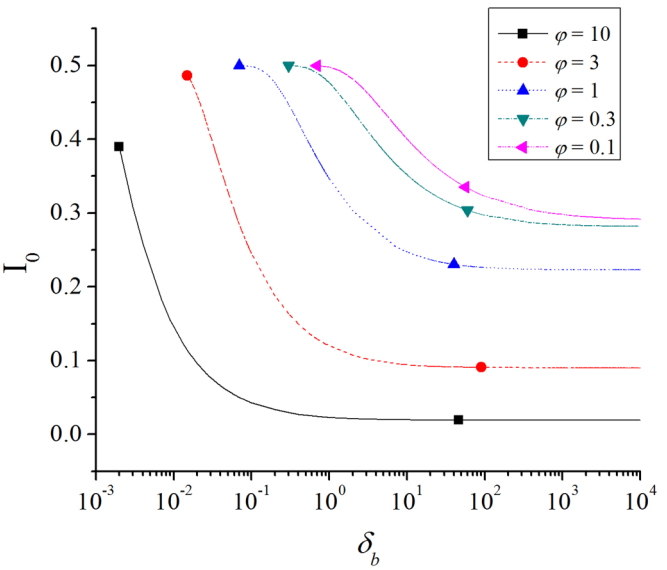

FIG. 10. The relationship between the total amount of the product I_0 and δ_b for various values of φ with Pe = 1.

VI. LARGE-TIME ASYMPTOTIC INNER SOLUTIONS

We now investigate the inner solution, which is only valid inside the reaction zone, i.e., only around the reaction front. We introduce the inner coordinate $Z = (\eta - \alpha)\tau^\sigma$ where $\sigma > 0$ so that as τ tends to infinity the term Z/τ^σ tends to zero, corresponding to η tending to α. Expanding the outer solutions around the reaction front, namely, $\eta = \alpha$, we obtain

$$a_L \to -\frac{UZ}{\tau^\sigma}, \quad b_L \to 0, \quad c_L \to W + \frac{W_L Z}{\tau^\sigma},$$
$$a_R \to 0, \quad b_R \to \frac{VZ}{\tau^\sigma}, \quad c_R \to W - \frac{W_R Z}{\tau^\sigma}.$$

We now seek an inner solution in a form that can match the outer solution by writing

$$a_I = \frac{\mathcal{A}^1(Z)}{\tau^\sigma}, \quad b_I = \frac{\mathcal{B}^1(Z)}{\tau^\sigma}, \quad c_I = W + \frac{\mathcal{C}^1(Z)}{\tau^\sigma}.$$

Substituting these expressions into system (7) yields

$$\sigma\mathcal{A}^1\tau^{-2\sigma} + \frac{1}{2}[(1-2\sigma)Z\tau^{-2\sigma} + \alpha\tau^{-\sigma}]\mathcal{A}^1_Z - \frac{(2\mathrm{Pe}-1)\tau^{-\sigma}\mathcal{A}^1_Z}{4(\alpha + Z\tau^{-\sigma})} = -\frac{\mathcal{A}^1_{ZZ}}{4} + \tau^{1-3\sigma}\mathcal{A}^1\mathcal{B}^1, \quad (36a)$$

$$\sigma\mathcal{B}^1\tau^{-2\sigma} + \frac{1}{2}[(1-2\sigma)Z\tau^{-2\sigma} + \alpha\tau^{-\sigma}]\mathcal{B}^1_Z - \frac{(2\delta_b\mathrm{Pe}-1)\tau^{-\sigma}\mathcal{B}^1_Z}{4\delta_b(\alpha + Z\tau^{-\sigma})} = -\frac{\mathcal{B}^1_{ZZ}}{4\delta_b} + \tau^{1-3\sigma}\mathcal{A}^1\mathcal{B}^1, \quad (36b)$$

$$\sigma\mathcal{C}^1\tau^{-2\sigma} + \frac{1}{2}[(1-2\sigma)Z\tau^{-2\sigma} + \alpha\tau^{-\sigma}]\mathcal{C}^1_Z - \frac{(2\delta_c\mathrm{Pe}-1)\tau^{-\sigma}\mathcal{C}^1_Z}{4\delta_c(\alpha + Z\tau^{-\sigma})} = -\frac{\mathcal{C}^1_{ZZ}}{4\delta_c} - \tau^{1-3\sigma}\mathcal{A}^1\mathcal{B}^1. \quad (36c)$$

In the large-time evolution, these equations consist of terms whose coefficients are powers of τ. In each equation the powers of τ present are -2σ, $-\sigma$, 0, and $1-3\sigma$. As $\sigma > 0$, we have $\sigma = 1/3$. The leading-order equations are

$$\mathcal{A}^1_{ZZ} = \frac{\mathcal{B}^1_{ZZ}}{\delta_b} = -\frac{\mathcal{C}^1_{ZZ}}{\delta_c} = 4\mathcal{A}^1\mathcal{B}^1.$$

The matching conditions for the inner solution with the left and right outer solutions are

$$\mathcal{A}^1 \to -UZ, \quad \mathcal{B}^1 \to 0, \quad \mathcal{C}^1 \to W_L Z, \quad \text{as} \quad Z \to -\infty,$$
$$\mathcal{A}^1 \to 0, \quad \mathcal{B}^1 \to VZ, \quad \mathcal{C}^1 \to -W_R Z \quad \text{as} \quad Z \to \infty.$$

By integrating the leading-order equation with respect to Z twice and using the conditions as $Z \to -\infty$ we obtain

$$\mathcal{A}^1 + UZ = \frac{\mathcal{B}^1}{\delta_b} = \frac{W_L Z - \mathcal{C}^1}{\delta_c},$$

then the condition as $Z \to \infty$ leads to

$$U = \frac{V}{\delta_b} = \frac{W_L + W_R}{\delta_c},$$

which is identical to the equation obtained in Sec. V by balancing the fluxes on each side of the reaction front.

Hence, we have shown that $\mathcal{B}^1 = \delta_b(\mathcal{A}^1 + UZ)$ and $\mathcal{C}^1 = W_L Z - \delta_c(\mathcal{A}^1 + UZ)$. Then using $\mathcal{A}^1_{ZZ} = 4\mathcal{A}^1\mathcal{B}^1$ we obtain a single ordinary differential equation for $\mathcal{A}^1$ given by $\mathcal{A}^1_{ZZ} = 4\delta_b\mathcal{A}^1(\mathcal{A}^1 + UZ)$. By scaling $Z = (4\delta_b U)^{-1/3}z$ and $\mathcal{A}^1 = (4\delta_b/U^2)^{-1/3}G$ we obtain

$$G_{zz} = G(z + G). \quad (37a)$$

The boundary conditions become

$$G \to -z \quad \text{as} \quad z \to -\infty, \quad (37b)$$
$$G \to 0 \quad \text{as} \quad z \to +\infty. \quad (37c)$$

The inner solution G can then be obtained numerically using Eq. (37). Once G has been obtained we have $\mathcal{A}^1 = (4\delta_b/U^2)^{-1/3}G$, $\mathcal{B}^1 = (4/\delta_b^2U^2)^{-1/3}(G + z)$, and $\mathcal{C}^1 = -\delta_c(4\delta_b/U^2)^{-1/3}[G + z - zW_L/(U\delta_c)]$. System (37) was analyzed in [13] where it was found that $G(-z) \equiv G(z) + z$ so that the differential equation in (37) can be written as $G_{zz} = G(z)G(-z)$ and so that $G_{zzz} = 0$ at $z = 0$ and thus G_{zz} is maximum at $z = 0$.

A. First moment of the reaction rate

We note that the reaction rate ab can be written as $\delta_b^{1/3}UG(G + z)/(4t)^{2/3}$. Now lets consider the first moment of the reaction rate,

$$\frac{r_f}{2\sqrt{\tau}} = \frac{\int_{-\infty}^{\infty} ab\eta^2 d\eta}{\int_{-\infty}^{\infty} ab\eta\, d\eta} = \frac{\int_{-\infty}^{\infty} ab(\alpha + Z\tau^{-1/3})^2 dZ}{\int_{-\infty}^{\infty} ab(\alpha + Z\tau^{-1/3})dZ}.$$

To evaluate this, a higher order expansion of the inner solutions is employed, as in [21], so that we have

$$a = \mathcal{A}^1\tau^{-1/3} + \mathcal{A}^2\tau^{-2/3} + \mathcal{A}^3\tau^{-1}$$

and

$$b = \mathcal{B}^1\tau^{-1/3} + \mathcal{B}^2\tau^{-2/3} + \mathcal{B}^3\tau^{-1}.$$

Then expanding r_f in large τ yields

$$\frac{r_f}{2\sqrt{\tau}} \to \alpha + \frac{P_2}{P_1\tau^{1/3}} + \frac{P_3 + \alpha Q_3}{\alpha P_1\tau^{2/3}} - \frac{(P_2 + \alpha Q_2)P_2}{\alpha P_1^2\tau^{2/3}}$$

where $P_1 = \langle\mathcal{A}^1\mathcal{B}^1\rangle$, $P_2 = \langle\mathcal{A}^1\mathcal{B}^1 Z\rangle$, $P_3 = \langle\mathcal{A}^1\mathcal{B}^1 Z^2\rangle$, $Q_2 = \langle\mathcal{A}^1\mathcal{B}^2 + \mathcal{A}^2\mathcal{B}^1\rangle$, and $Q_3 = \langle\mathcal{A}^1\mathcal{B}^2 + \mathcal{A}^2\mathcal{B}^1 Z\rangle$, where $\langle f, g\rangle = \int_{-\infty}^{\infty} fg\, dz$. Thus to first order we have

$$\frac{r_f}{2\sqrt{\tau}} \to \alpha + \frac{\langle\mathcal{A}^1\mathcal{B}^1 Z\rangle}{\langle\mathcal{A}^1\mathcal{B}^1\rangle\tau^{1/3}}.$$

As this only involves the leading-order, solution we can express this in terms of the function G as

$$\frac{r_f}{2\sqrt{\tau}} \to \alpha + \frac{1}{(4\delta_b U\tau)^{1/3}}\frac{\int_{-\infty}^{\infty} G_{zz} z\, dz}{\int_{-\infty}^{\infty} G_{zz} dz}.$$

However, using the boundary conditions in system (37) we have $\int_{-\infty}^{\infty} G_{zz}dz = [G_z]_{-\infty}^{\infty} = 1$ and $\int_{-\infty}^{\infty} G_{zz}zdz = [G_z z - G]_{-\infty}^{\infty} = 0$, so $P_2 = 0$. Thus,

$$\frac{r_f}{2\sqrt{\tau}} \to \alpha + O(\tau^{-2/3}) \quad (38)$$

and the first moment of the reaction rate corresponds to the point $r_f = 2\alpha\sqrt{\tau} + O(\tau^{-1/6})$, i.e., the point where the large-time asymptotic outer solutions satisfy $a = b = 0$.

Hence, just as in the case of planar reaction fronts, for the reaction $A + B \to C$ the local maximum in the reaction rate and the first moment of the reaction rate coincide in the large time asymptotic limit (at $z = 0$ in the inner coordinate system).

B. Width of the reaction front

Now lets consider the second moment of the reaction rate,

$$\frac{w_f^2 + r_f^2}{4\tau} = \frac{\int_0^\infty ab\eta^3 d\eta}{\int_0^\infty ab\eta\, d\eta} = \frac{\int_{-\infty}^\infty ab(\alpha + Z\tau^{-1/3})^3 dZ}{\int_{-\infty}^\infty ab(\alpha + Z\tau^{-1/3}) dZ}.$$

Then expanding r_f in large τ yields

$$\frac{w_f^2 + r_f^2}{4\tau} \to \alpha^2 + \frac{2\alpha P_2}{P_1\tau^{1/3}} + \frac{3P_3 + 2\alpha Q_3}{P_1\tau^{2/3}} - \frac{2(P_2 + \alpha Q_2)P_2}{\alpha P_1^2\tau^{2/3}}.$$

Hence, using the result for r_f, we obtain

$$\frac{w_f^2}{4\tau} \to \frac{P_3}{P_1\tau^{2/3}} - \frac{P_2^2}{P_1^2\tau^{2/3}}.$$

Thus, using the results in the previous subsection that $P_2 = 0$, we obtain

$$w_f^2 \to 4\tau^{1/3}\frac{\langle \mathcal{A}^1\mathcal{B}^1 Z^2\rangle}{\langle \mathcal{A}^1\mathcal{B}^1\rangle}.$$

Again, as this only involves the leading-order solution, we can express this in terms of the function G as

$$w_f^2 \to \frac{(4\tau)^{1/3}}{(\delta_b U)^{2/3}}\frac{\int_{-\infty}^\infty G_{zz} z^2 dz}{\int_{-\infty}^\infty G_{zz} dz}.$$

Hence, using the integral results we obtain

$$w_f \to \frac{2^{1/3}\sqrt{\Phi}}{(\delta_b U)^{1/3}}\tau^{1/6}, \tag{39}$$

where $\Phi = \int_{-\infty}^\infty G_{zz} z^2 dz$. Numerically, the authors of [32] found that $\Phi \approx 1.90250$.

We note that although the equation for w_f appears to be the same as what one obtains for a planar reaction front (see [32]), the term U is different. In the large Pe limit, using $\alpha = \sqrt{\mathrm{Pe}} + \psi/\sqrt{2}$, we find that

$$U \to \frac{2\sqrt{2}e^{-\psi^2}}{\sqrt{\pi}\,\mathrm{erfc}(-\psi)},$$

which is $\sqrt{2}$ times larger than the term U given in [32]. Thus in the large-time asymptotic limit for large Pe, the concentration gradients around the radial reaction front are $\sqrt{2}$ times larger those of a planar reaction front and the width of a radial reaction front is $1/2^{1/6}$ of the width of a planar reaction front.

VII. CONCLUSIONS

This article considers the analytical, numerical, and small- and large-time asymptotic solutions of the reaction equation $A + B \to C$ in a Hele-Shaw cell where a reactant solution A is injected as a point source into a reactant B. A polar-coordinate system is employed to accurately model the reaction line as it extends from the point source.

A Crank-Nicolson numerical method is employed to ascertain numerical solutions, showing that diffusion dominates over advection in the early stages of the slow flow regime. Advection is shown to dominate proceedings in the fast flow regime and no overall control is displayed in the moderate flow regime. In late stages of the experiment, the slow flow regime illustrates sharp concentration gradients near the center of the sample, the moderate flow regime shows the maximum concentration of the product moving away from the center of the sample, and the fast flow regime illustrates that the concentration gradients of all species tend to zero away from the reaction front, resembling the concentration profiles of the planar reaction problem.

Small- and large-time asymptotic solutions are found for a variety of special cases, each of which closely matches the numerical solutions found using the finite-differences scheme. The effects of the parameters related to the Péclet number and the molecular diffusion coefficients are also investigated.

It would be of great interest if previous $A + B \to C$ experiments in planar geometries could be reinvestigated in radial geometries and compared with the results found herein. For example, experiments using Cu^{2+} ions with disodium ethyl bis (5-tetrazolylazo) acetate trihydrate in [14,33] or Cu^{2+} ions with calcium green in [34,35], which use a variety of species concentrations and molecular diffusion coefficients, could be reanalyzed to confirm the analysis within.

This theory could be applied in many experiments where the consumption of reagent can lead to unstable density distortions such as density fingering, which has not been considered here. For most liquids, viscosities vary very slowly with concentration changes, so in a dilute system it is usually valid to ignore viscosity variations and so viscous fingering instabilities can be neglected. Furthermore, in dilute systems buoyancy instabilities will have no effect for small to intermediate times. The actual length of time the solution remains valid is expected to strongly depend on the flow rates, diffusion coefficients, concentrations, and the solutal expansion coefficients of the species. Nevertheless, the length of time for which the solutions are valid could be determined by performing a linear stability analysis on the spatially varying time-dependent profiles to determine when the integral of the real part of the instantaneous growth of the instability becomes order 1, at this point the solutions are no longer valid. This remains a worthwhile exercise for the interested reader.

ACKNOWLEDGMENT

P.M.J.T. would like to thank Anne De Wit for fruitful discussions.

APPENDIX A: LOWER LIMIT OF $\Gamma(a, x)$

Consider

$$G = \Gamma(\mathrm{Pe}, y^2),$$

which by the definition of the incomplete gamma function implies that

$$G_y = -2y^{2\mathrm{Pe}-1}e^{-y^2}.$$

If Pe is very small, then there is a boundary layer near $y = 0$. Thus if we consider $0 < y \ll 1$ and expand the exponential term we obtain

$$G_y = -2y^{2\mathrm{Pe}-1} + 2y^{2\mathrm{Pe}+1} - \frac{y^{2\mathrm{Pe}+3}}{2} + \cdots,$$

which can be directly integrated to yield

$$G = \Gamma(\mathrm{Pe}) - \frac{y^{2\mathrm{Pe}}}{\mathrm{Pe}} + \frac{y^{2\mathrm{Pe}+2}}{\mathrm{Pe}+1} - \frac{y^{2\mathrm{Pe}+4}}{4\mathrm{Pe}+8} + \cdots,$$

where the integration constant is $\Gamma(\mathrm{Pe})$ since the remaining terms in the expansion are all zero at $y = 0$. Hence,

$$\Gamma(\mathrm{Pe}) - \Gamma(\mathrm{Pe}, y^2) = \frac{y^{2\mathrm{Pe}}}{\mathrm{Pe}} - \frac{y^{2\mathrm{Pe}+2}}{\mathrm{Pe}+1} + \frac{y^{2\mathrm{Pe}+4}}{4\mathrm{Pe}+8} + \cdots \quad \text{(A1)}$$

if both Pe and y are small. One notes that the term $y^{2\mathrm{Pe}}$ can be written as $\exp[2\mathrm{Pe}\ln(y)] \approx 1 + 2\mathrm{Pe}\ln(y)$ as Pe is small.

In this study we shall also use the limit

$$\Gamma(x) \to \frac{1}{x} - \gamma + \left(\frac{\pi^2}{12} + \frac{\gamma^2}{2}\right)x + \cdots \quad \text{(A2)}$$

as x tends to zero, where γ is Euler's constant, which is approximately given by 0.5772156649.

APPENDIX B: UPPER LIMIT OF $\Gamma(a, x)$

We recall that the solution to the equation

$$-2\eta a_\eta + (2\mathrm{Pe} - 1)\frac{a_\eta}{\eta} = a_{\eta\eta}$$

is $a = \Gamma(\mathrm{Pe}, \eta^2)/\Gamma(\mathrm{Pe})$. This function will be approximated by extending the expansion by Tan and Homsy [36]. We substitute $\eta = \sqrt{\mathrm{Pe}} + \xi/\sqrt{2}$ into the differential equation and expand in large Pe to obtain

$$\frac{a_{\xi\xi}}{a_\xi} = -2\xi + (\xi^2 - 1)\left[\frac{1}{\sqrt{2\mathrm{Pe}}} - \frac{\xi}{2\mathrm{Pe}} + \cdots\right].$$

This can be integrated to yield

$$a_\xi = c_1 \exp\left(-\xi^2 + \left[\frac{\xi^3 - 3\xi}{3\sqrt{2\mathrm{Pe}}} - \frac{\xi^4 - 2\xi^2}{8\mathrm{Pe}} + \cdots\right]\right).$$

Then expanding in large Pe yields

$$a_\xi = c_1 e^{-\xi^2}\left[1 + \frac{\xi^3 - 3\xi}{3\sqrt{2\mathrm{Pe}}} + \frac{36\xi^2 - 21\xi^4 + 2\xi^6}{72\mathrm{Pe}} + \cdots\right].$$

By integrating this and using the boundary conditions that a tends to 1 as ξ tends to $-\infty$ and a tends to zero as ξ tends to ∞, we obtain the approximate solution

$$a = \frac{\mathrm{erfc}(\xi)}{2} + \frac{e^{-\xi^2}}{6\sqrt{\pi}}\left[\frac{\xi^2 - 2}{\sqrt{2\mathrm{Pe}}} + \frac{6\xi - 8\xi^3 + \xi^5}{12\mathrm{Pe}} + \cdots\right] \quad \text{(B1)}$$

as Pe tends to infinity. Numerically, one finds that the second-order expansion, shown in Eq. (B1), along with a first-order expansion and a zeroth-order expansion have errors of approximately $0.0086/\mathrm{Pe}^{3/2}$, $0.0128/\mathrm{Pe}$, and $0.133/\sqrt{\mathrm{Pe}}$, respectively, as Pe tends to infinity.

As an aside, one notes that a slight improvement to the zeroth-order approximation is

$$a = \frac{1}{2}\mathrm{erfc}\left(\xi + \frac{1}{3\sqrt{2\mathrm{Pe}}}\right),$$

which has an error approximately given by $0.025/\sqrt{\mathrm{Pe}}$.

In this study we shall also use the limit

$$\Gamma(x) \to \sqrt{2\pi}e^{-x}x^{x-\frac{1}{2}}\left(1 + \frac{1}{12x} + \cdots\right) \quad \text{(B2)}$$

as x tends to infinity, from Eq. (6.1.37) from Abramowitz and Stegun [30].

APPENDIX C: COMPARING PLANAR AND RADIAL REACTION FRONTS FOR FAST FLOWS

Let us next consider the transport equations (7) for a radial reaction front in a coordinate system moving with the contact line $\xi = \sqrt{2}(\eta - \sqrt{\mathrm{Pe}})$. The transport equations become

$$\tau a_\tau - (\sqrt{2\mathrm{Pe}} + \xi)\frac{a_\xi}{2} + \frac{(2\mathrm{Pe} - 1)a_\xi}{2(\sqrt{2\mathrm{Pe}} + \xi)} = \frac{a_{\xi\xi}}{2} - ab\tau,$$

$$\tau b_\tau - (\sqrt{2\mathrm{Pe}} + \xi)\frac{b_\xi}{2} + \frac{(2\mathrm{Pe} - 1/\delta_b)b_\xi}{2(\sqrt{2\mathrm{Pe}} + \xi)} = \frac{b_{\xi\xi}}{2\delta_b} - ab\tau,$$

$$\tau c_\tau - (\sqrt{2\mathrm{Pe}} + \xi)\frac{c_\xi}{2} + \frac{(2\mathrm{Pe} - 1/\delta_c)c_\xi}{2(\sqrt{2\mathrm{Pe}} + \xi)} = \frac{c_{\xi\xi}}{2\delta_c} + ab\tau.$$

For fast flow rates we expand this system in large Pe to obtain

$$\tau a_\tau - \xi a_\xi = \frac{a_{\xi\xi}}{2} - ab\tau,$$

$$\tau b_\tau - \xi b_\xi = \frac{b_{\xi\xi}}{2\delta_b} - ab\tau,$$

$$\tau c_\tau - \xi c_\xi = \frac{c_{\xi\xi}}{2\delta_c} + ab\tau,$$

where corrections of the order $O(\mathrm{Pe}^{-1/2})$ have been neglected. If we then seek a similarity solution, so that the solution becomes independent of τ, then one obtains

$$-\xi a_\xi = \frac{a_{\xi\xi}}{2}, \quad -\xi b_\xi = \frac{b_{\xi\xi}}{2\delta_b}, \quad -\xi c_\xi = \frac{c_{\xi\xi}}{2\delta_c}.$$

which is identical to the system of similarity equations that one obtains for a planar reaction front.

Hence, in the large-Péclet-number limit, in a reference frame moving with the injected fluid, the radial reaction front behaves just like the planar reaction front when a similarity solution exists. Such solutions exist in both the small- and large-time asymptotic limits, and hence as Pe tends to infinity, we find that

$$r_m = r_c + x_m/\sqrt{2}, \quad r_f = r_c + x_f/\sqrt{2}, \quad \text{(C1)}$$

where r_m is the location where the reaction rate is maximum, r_f is the first moment of the reaction rate for a radial reaction front, and x_m and x_f are the corresponding quantities for a planar reaction front. Thus the distance between the radial reaction front and the contact line is equal to the distance that a planar reaction front travels divided by $\sqrt{2}$.

[1] S. A. Rice, *Diffusion-Limited Reactions*, 1st ed. (Elsevier Science, Amsterdam, 1985).
[2] D. ben-Avraham and S. Havlin, *Diffusion and Reactions in Fractals and Disordered Systems* (Cambridge University Press, Cambridge, 2000).
[3] A. Zalts, C. El Hasi, D. Rubio, A. Urena, and A. D'Onofrio, Phys. Rev. E **77**, 015304(R) (2008).
[4] C. Almarcha, P. M. J. Trevelyan, P. Grosfils, and A. De Wit, Phys. Rev. Lett. **104**, 044501 (2010).
[5] C. Almarcha, P. M. J. Trevelyan, L. Riolfo, A. Zalts, C. El Hasi, A. D'Onofrio, and A. De Wit, J. Phys. Chem. Lett. **1**, 752 (2010).
[6] C. Almarcha, Y. R'Honi, Y. De Decker, P. M. J. Trevelyan, K. Eckert, and A. De Wit, J. Phys. Chem. B **115**, 9739 (2011).
[7] Y. Shi and K. Eckert, Chem. Eng. Sci. **61**, 5523 (2006).
[8] A. Riaz, M. Hesse, H. A. Tchelepi, and F. M. Orr, Jr., J. Fluid Mech. **548**, 87 (2006).
[9] K. Eckert, M. Acker, and Y. Shi, Phys. Fluids **16**, 385 (2004).
[10] D. A. Bratsun, Y. Shi, K. Eckert, and A. De Wit, Europhys. Lett. **69**, 746 (2005).
[11] L. Rongy, P. M. J. Trevelyan, and A. De Wit, Phys. Rev. Lett. **101**, 084503 (2008).
[12] G. Venzl, J. Chem. Phys. **85**, 2006 (1986).
[13] L. Gálfi and Z. Rácz, Phys. Rev. A **38**, 3151 (1988).
[14] Y.-E. L. Koo and R. Kopelman, J. Stat. Phys. **65**, 893 (1991).
[15] A. Yen and R. Kopelman, Phys. Rev. E **56**, 3694 (1997).
[16] Z. Koza, J. Stat. Phys. **85**, 179 (1996).
[17] M. Sinder and J. Pelleg, Phys. Rev. E **62**, 3340 (2000).
[18] S. Cornell, M. Droz, and B. Chopard, Phys. Rev. A **44**, 4826 (1991).
[19] S. Cornell and M. Droz, Phys. Rev. Lett. **70**, 3824 (1993).
[20] S. Cornell, Z. Koza, and M. Droz, Phys. Rev. E **52**, 3500 (1995).
[21] P. M. J. Trevelyan, Phys. Rev. E **79**, 016105 (2009).
[22] P. M. J. Trevelyan, Phys. Rev. E **80**, 046118 (2009).
[23] H. Taitelbaum, S. Havlin, J. E. Kiefer, B. Trus, and G. H. Weiss, J. Stat. Phys. **65**, 873 (1991).
[24] H. Taitelbaum, Y.-E. L. Koo, S. Havlin, R. Kopelman, and G. H. Weiss, Phys. Rev. A **46**, 2151 (1992).
[25] I. Hecht and H. Taitelbaum, Phys. Rev. E **74**, 012101 (2006).
[26] H. Taitelbaum and Z. Koza, Physica A **285**, 166 (2000).
[27] F. Brau, G. Schuszter, and A. De Wit, Phys. Rev. Lett. **118**, 134101 (2017).
[28] G. Schuszter, F. Brau, and A. De Wit, Environ. Sci. Technol. Lett. **3**, 156 (2016).
[29] B. M. Shipilevsky, Phys. Rev. E **70**, 032102 (2004).
[30] M. Abramowitz and I. A. Stegun, *Handbook of Mathematical Functions* (Dover, New York, 1972).
[31] E. T. Whittaker and G. N. Watson, *A Course of Modern Analysis* (Cambridge University Press, Cambridge, 1927).
[32] P. M. J. Trevelyan, D. E. Strier, and A. De Wit, Phys. Rev. E **78**, 026122 (2008).
[33] S. H. Park, S. Parus, R. Kopelman, and H. Taitelbaum, Phys. Rev. E **64**, 055102(R) (2001).
[34] C. N. Baroud, F. Okkels, L. Ménétrier, and P. Tabeling, Phys. Rev. E **67**, 060104(R) (2003).
[35] S. H. Park, H. Peng, R. Kopelman, and H. Taitelbaum, Phys. Rev. E **75**, 026107 (2007).
[36] C. T. Tan and G. M. Homsy, Phys. Fluids **30**, 1239 (1987).